Pure Appl. Chem., Vol. 82, No. 10, pp. 1927–1941, 2010.
doi:10.1351/PAC-CON-09-10-28

Structure, solvation, and acid–base property in ionic liquids*

Shin-ichi Ishiguro‡, Yasuhiro Umebayashi, Ryo Kanzaki, and Kenta Fujii

Department of Chemistry, Faculty of Science, Kyushu University, Hakozaki, Higashi-ku, Fukuoka, 812-8581, Japan

Abstract: Ionic liquids (ILs) are expected to have specific properties as solvents for chemical reactions in view of solution chemistry. Among physicochemical properties, liquid structure, acid–base, and electron-pair donating and accepting abilities of solvent play a crucial role in ion-solvation and acid–base, metal-ion complexation, and electrochemical reactions. Various types of ILs have been developed, and among others, the bis(trifluoromethanesulfonyl)amide ($TFSA^-$)-based ILs are extensively used. $TFSA^-$ is a flexible molecule to give two stable conformers, *cis* (C1) and *trans* (C2), which are present in equilibrium in the liquid state. The conformational equilibrium shifts upon solvation to the metal ion. This is quantitatively studied to obtain thermodynamic parameters of conformational change from C2 to C1 in the bulk and in the solvation sphere of the lithium ion. On the other hand, with ethylammonium nitrate (EAN), a typical protic IL, it is revealed that the ammonium group is hydrogen-bonded with three nitrate ions to form a heterogeneous liquid structure. The solvent acid–base property of EAN and acid dissociation reaction in EAN have been quantitatively revealed, and the results will be discussed in comparison with those in normal molecular solvents.

Keywords: acid–base; conformation; ionic liquids; solution chemistry; solvation; bis(trifluoromethanesulfonyl)amide (TFSA).

INTRODUCTION

Solute–solvent and solvent–solvent interactions are essential in solution chemistry. Solute–solvent interaction, or solvation of solute ions or molecules, play a crucial role in reactions, such as dissolution of salts, and acid–base, metal-ion complexation, redox reactions, etc. in solution, because solute ions and molecules are solvated, and ligating solvent molecules desolvate solutes upon reaction [1]. Here, electron-pair donating and accepting abilities of solvent play a significant role in determining the strength of solvation of cation and anion, respectively [2]. Solvent–solvent interaction or liquid structure of solvent also plays an important role in reactions in solution, because liberated solvent molecules upon reaction are transferred, and finally accommodated in the bulk liquid structure [3]. It is known that protic solvents capable of hydrogen-bonding, like water, tend to form a strong liquid structure, whereas the liquid structure in aprotic solvents is rather weak. Reaction entropy in a given solvent strongly depends on the strength of liquid structure of the solvent. This is because translational and rotational motions of solvent are strongly hindered when it is bound to an ion, whereas it is significantly encouraged

*Paper based on a presentation at the 31st International Conference on Solution Chemistry (ICSC-31), 21–25 August 2009, Innsbruck, Austria. Other presentations are published in this issue, pp. 1855–1973.
‡Corresponding author

upon desolvation or liberation from the ion, leading to an increase in entropy. However, note that solvent molecules again lose the freedom of motion when it is accommodated in a solvent structure in the bulk. The extent of entropy loss may depend on the strength of liquid structure. Entropy loss may be small in aprotic solvents with weak solvent–solvent interactions, whereas it is large to offset entropy obtained upon desolvation in protic solvent with strong solvent–solvent interactions. Solute–solvent and solvent–solvent interactions have been extensively studied in normal molecular solvents so far [4], but not in ionic liquids (ILs).

Room-temperature ILs, composed of bulky organic cations and inorganic anions, are attracting attention as novel solvents in various fields of chemistry, as well as applications [5–7]. Physicochemical properties of ILs might be compared with those of conventional molten salts and molecular liquids. ILs are practically nonvolatile and thus nonflammable like conventional molten salts, whereas they show a surprisingly low melting point like molecular liquids. The melting point T_{melt} at a given pressure is given by $T_{melt} = \Delta_{melt}H^\circ/\Delta_{melt}S^\circ$, where $\Delta_{melt}H^\circ$ and $\Delta_{melt}S^\circ$ stand for the enthalpy and entropy of melting, respectively. Evidently, low T_{melt} is derived from small $\Delta_{melt}H^\circ$, together with large $\Delta_{melt}S^\circ$. Bulky and/or nonsymmetrical molecular structures may lower the lattice energy of ILs in the solid state to lead to small $\Delta_{melt}H^\circ$, and flexible structures accompanying conformational changes may lead to large $\Delta_{melt}S^\circ$.

The liquid structure of ILs seems to be heterogeneous, unlike that of molecular solvents [8–11]. An organic cation usually involves nonpolar alkyl groups, like a surfactant molecule, and it is suggested that the alkyl group tends to aggregate to form nonpolar domains in the liquid state, and polar groups also favorably interact to form polar domains. ILs are thus considered to be a mixture of molecular solvents that are not miscible at a molecular level. The heterogeneous liquid structure of ILs might bring about specific solvent properties, not only physicochemical properties of neat solvents but also those related to solute reactivities in ILs, like micellar solutions [12].

With reactions in solution, the acid or base strength of a solute depends on the acid–base property of solvent [13–15]. Also, complexation and redox reactions of solute species depend on the electron-pair donating and accepting properties of solvent [16]. However, the acid–base property of ILs is not satisfactorily established yet in terms of solution chemistry. Also, the electron-pair donating and accepting properties of solvent are not established yet. With ILs, we know little about what are already established for normal molecular liquids. Therefore, to elucidate solute–solvent and solvent–solvent interactions in ILs, we have been studying molecular conformation and liquid structure of some protic and aprotic ILs, as well as acid–base properties and solvation of metal ions [17–34]. Here, we review our recent results on the conformational equilibrium of bis(trifluoromethanesulfonyl)amide ($TFSA^-$) anion, and its solvation to the metal ion. We also demonstrate the solvent acid–base property of ethylammonium nitrate (EAN) and the acid dissociation of α-alanine in EAN.

METAL-ION SOLVATION

In an IL, metal ions interact with solvent anions, and metal–solvent bond may be formed through the electron-pair donating atom of anion. Although $TFSA^-$ is a conjugate base of a super acid, i.e., the electron-pair donating ability of the O-donor atom is very weak; $TFSA^-$ coordinates to the metal ion in ILs. This is indeed confirmed by Raman spectra of $M(TFSA)_2$ (M = Mn and Zn) solutions in 1-ethyl-3-methylimidazolium (EMI^+) $TFSA^-$ [35]. As seen in Fig. 1, with increasing concentration of the metal ion, the band intensity at around 740 cm^{-1} decreases and a new band appears at a higher wave number. The decreasing band is ascribed to the stretching $\nu_{S–N–S}$ + bending δ_{CF3} vibration of free $TFSA^-$ in the bulk, and the increasing band to the corresponding band of $TFSA^-$ bound to the metal ion. To evaluate the solvation number, Raman spectra were deconvoluted into two bands, free and bound, using the pseudo-Voigt function, and integrated intensity was extracted for each band. The solvation number n can be obtained by analyzing data according to

$$I_f/c_M = J_f(c_{TFSA}/c_M - n) \quad (1)$$

where I_f, J_f, c_M, and c_{TFSA} stand for the integrated intensity, Raman scattering coefficient of free $TFSA^-$, and concentrations of the metal ion and $TFSA^-$, respectively, in solution. Plots of I_f/c_M against c_{TFSA}/c_M give a straight line, and it is found that the solvation number is 3.0 for both Mn^{2+} and Zn^{2+} ions. The same conclusion is also obtained for Ni^{2+} and Co^{2+}. The color of $Ni(TFSA)_2$ and $Co(TFSA)_2$ solutions in EMI^+TFSA^- is not the same as that in water, but is rather similar to that in *N*,*N*-dimethylacetamide (DMA). It has already been established that these metal ions are six-solvated with a distorted octahedral structure in DMA. It is thus supposed that three $TFSA^-$ ions chelate, as a bidentate O donor ligand, to the transition-metal(II) ions, and the octahedral six-coordinate structure is distorted. This is indeed found in the crystal structure of metal-$TFSA^-$ salts [36].

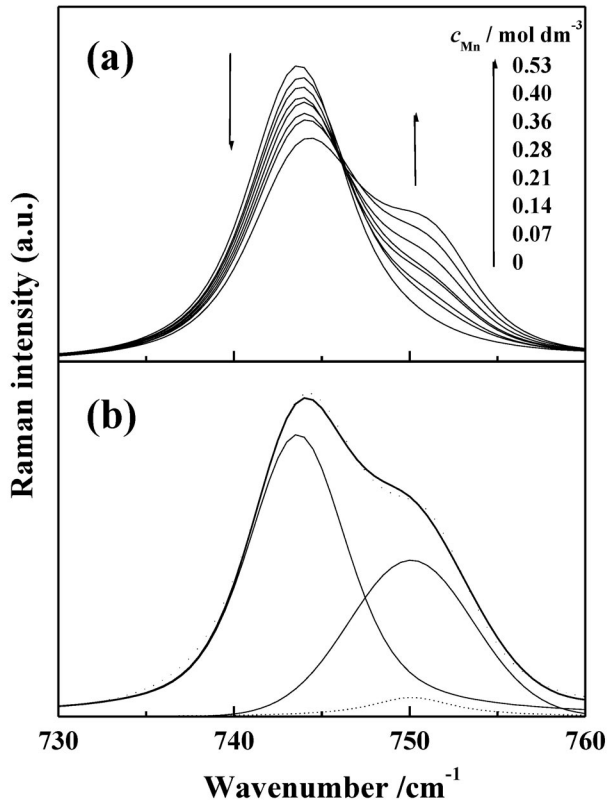

Fig. 1 Variation of a Raman band ($\nu_{SNS} + \delta_{CF3}$) of $TFSA^-$ with increasing concentration of the metal ion in $Mn(TFSA)_2$ solution of EMI^+TFSA^- (a), and deconvoluted bands of TFSA (solid line) and EMI^+ (dotted line), together with the observed (solid line) and corresponding calculated (dotted line) spectra (b).

The solvation number of the lithium ion in EMI^+TFSA^- has also been obtained [37]. The value is two, which may be expected if we take into account that the lithium ion is usually four-coordinated in normal oxygen-donor solvents. We will discuss the solvation of $TFSA^-$ around the lithium ion in detail in the following section.

CONFORMATIONAL EQUILIBRIUM

Solvent *N*,*N*-dimethylpropionamide (DMPA) involves two conformers, planar-*cis* and nonplanar staggered, in equilibrium in the liquid state. The former is favorable in the bulk, but the latter is preferred in the solvation sphere of a small metal ion [38]. This is unusual, because organic solvents usually have rigid molecular structures. On the other hand, the reverse is the case for ILs. ILs are usually flexible and can easily change their conformation. Among ILs, $TFSA^-$-based ILs show a relatively low melting point. Indeed, $TFSA^-$ is a flexible molecule and easily changes its conformation, and it is found that C1 and C2 conformers shown in Fig. 2 are relatively stable, according to theoretical calculation [20,38]. With regard to the structure $[F_3CS(O)_2NS(O)_2CF_3]^-$ of $TFSA^-$, the SNS linkage is not linear to give a plane, and the terminal CF_3 group can rotate around the N–S bond. Here, two CF_3 groups locate *cis* against the SNS plane in the C1 conformer, and *trans* in the C2 conformer. Some structural parameters optimized by density functional theory (DFT) calculations with the B3LYP/6-311+G(3df) are shown in Table 1. Interestingly, dipole moment is significantly larger for C1 than C2. Potential energy surface for conformational change is shown in Fig. 3, which is calculated by fixing one CF_3 group at a given dihedral C–S–N–S angle of $\theta = 90°$ (nonplanar, filled circle) or 180° (planar, open circle), and another CF_3 group is rotated. As seen in Fig. 3, the global minimum appears at $\theta = 90°$ for the C2 conformer. Also, we see two rotational barriers. One is low, but another is high, and it is thus supposed that the CF_3 group cannot freely rotate but swing to change conformation at room temperature.

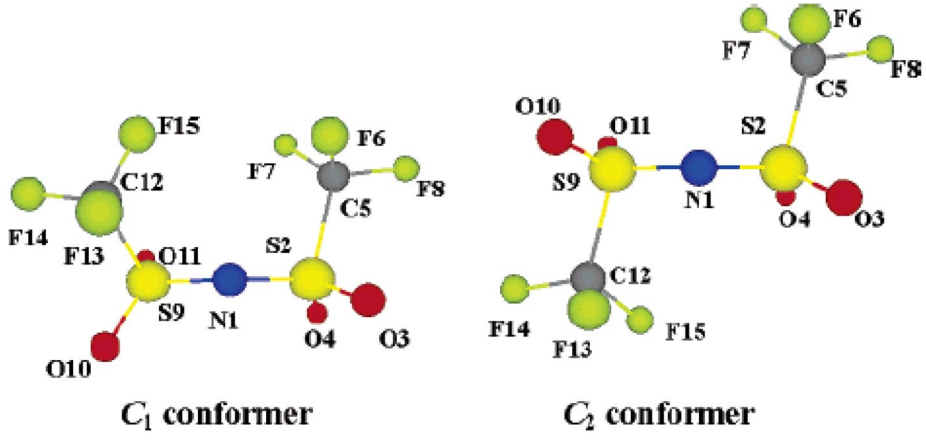

Fig. 2 Structure of C1 (*cis*) and C2 (*trans*) conformers of $TFSA^-$.

Table 1 Some structural parameters of the C1 and C2 conformers of $TFSA^-$, optimized by DFT calculations using B3LYP/6-311+G(3df). The label of atoms is shown in Fig. 2.

	C1	C2
Dipole moment/D	4.404	0.301
Angle/°		
S–N–S	128.4	127.8
Dihedral angle/°		
S2–N1–S9–C12	–88.2	93.7
S9–N1–S2–C5	130.7	93.7
C5–S2–S9–C12	42.5	175.6

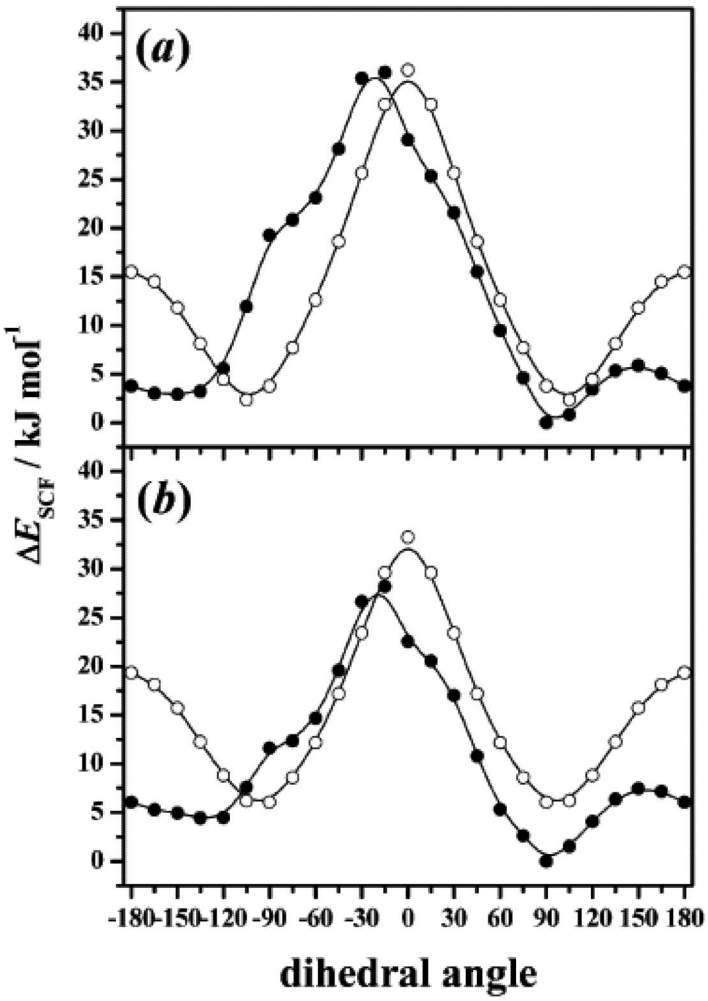

Fig. 3 Potential energy surface for the conformational change of $TFSA^-$ as a function of the C–S–N–S dihedral angle, calculated using theories HF/6-31G(d) (a) and B3LYP/6-31G(d) (b). Another C–S–N–S dihedral angle is fixed at 90º (●) or 180º (○).

Evidence of conformational equilibrium is indeed obtained by Raman spectra in Fig. 4. Raman spectrum at around 400 cm^{-1} gives two peaks, which cannot be explained in terms of a single conformer, because both C1 and C2 conformers give a single band at around 400 cm^{-1}, which appears at higher and lower frequency, respectively, as seen in theoretical Raman bands. Furthermore, relative intensity of the two bands varies with rising temperature, suggesting the presence of conformational equilibrium. Here, Raman intensity which has been normalized using a single band of 1-butyl-3-methyl imidazolium (BMI^+) ion as an internal standard is further corrected for Boltzman distribution and density with temperature. Raman spectra are then deconvoluted into single bands. The intensity of a single band is given as $I = Jc$, i.e., product of the scattering coefficient J and concentration c of a conformer. On the basis of the relationship, $-R\ln K = \Delta H°/T + \Delta S°$, where K, $\Delta H°$m and $\Delta S°$ stand for equilibrium constant, enthalpy, and entropy for the reaction $C_2 \rightleftharpoons C_1$, we obtain the following equation as

$$-R\ln(I_{C1}/I_{C2}) = \Delta H°/T - \Delta S° - R\ln(J_{C1}/J_{C2}) \quad (2)$$

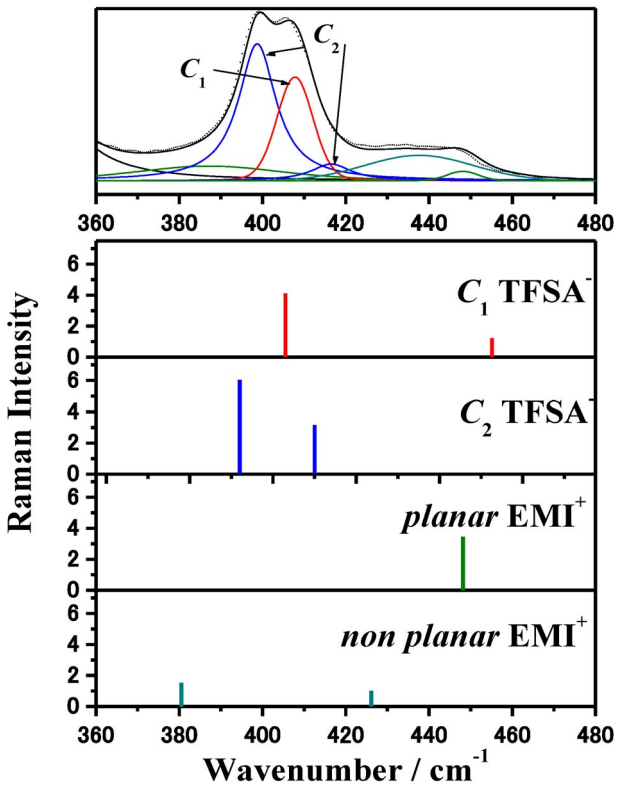

Fig. 4 Observed and theoretical Raman bands of EMI^+TFSA^- in the range 360–480 cm^{-1}.

The $-R\ln(I_{C1}/I_{C2})$ values are then plotted against reciprocal temperature, and the slope gives the enthalpy $\Delta H°$ for conformational change from C2 to C1. The enthalpy thus obtained in EMI^+TFSA^- is 3.5 kJ mol^{-1}. The positive enthalpy is consistent with the conclusion obtained from theoretical calculation that the C2 conformer gives the global minimum.

It has been shown that $TFSA^-$ solvates the metal ion. Let's consider the lithium ion in BMI^+TFSA^-, in which two $TFSA^-$ solvate the metal ion. Here, if we take into account the conformation of $TFSA^-$, three types of the solvate ion, C1C1, C1C2, and C2C2, as shown in Fig. 5, may be possible. However, they show similar energies according to theoretical calculations, and direct experimental investigation in solution is thus indispensable to conclude which is the most favorable solvate. Raman spectra measured for BMI^+TFSA^- with and without containing lithium ion show quite different behavior with raising temperature. As seen in Fig. 6, in neat solvent without the lithium ion, the band at a lower-frequency side (C2) decreases, whereas the band at a higher-frequency side (C1) remains almost unchanged. On the other hand, in solution containing 0.171 mole fraction of $TFSA^-$ ions bound to the metal ion, both bands decrease. If the conformational equilibrium is established in the coordination sphere, as well as in the bulk, the apparent enthalpy $\Delta H_{app}°$ experimentally obtained can be represented as the sum of enthalpies weighted by mole fraction of $TFSA^-$ in the bulk and in the coordination sphere as follows:

$$\Delta H_{app}° = x_{bulk}\Delta H_{bulk}° + x_{bound}\Delta H_{bound}° \quad (3)$$
$$(x_{bulk} + x_{bound} = 1)$$

Here, mole fractions of $TFSA^-$ in the bulk and in the coordination sphere, x_{bulk} and x_{bound}, respectively, can be evaluated on the basis of the solvation number of two for $TFSA^-$ and the concentration of the

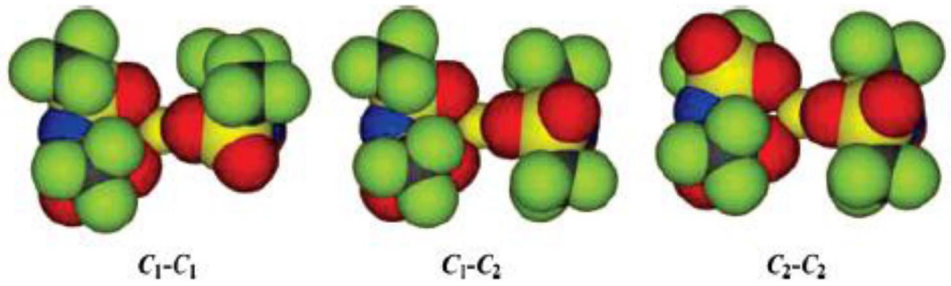

Fig. 5 Optimized structures of $Li(TFSA)_2^-$ with three types of $TFSA^-$ conformers, C1–C1, C1–C2, and C2–C2.

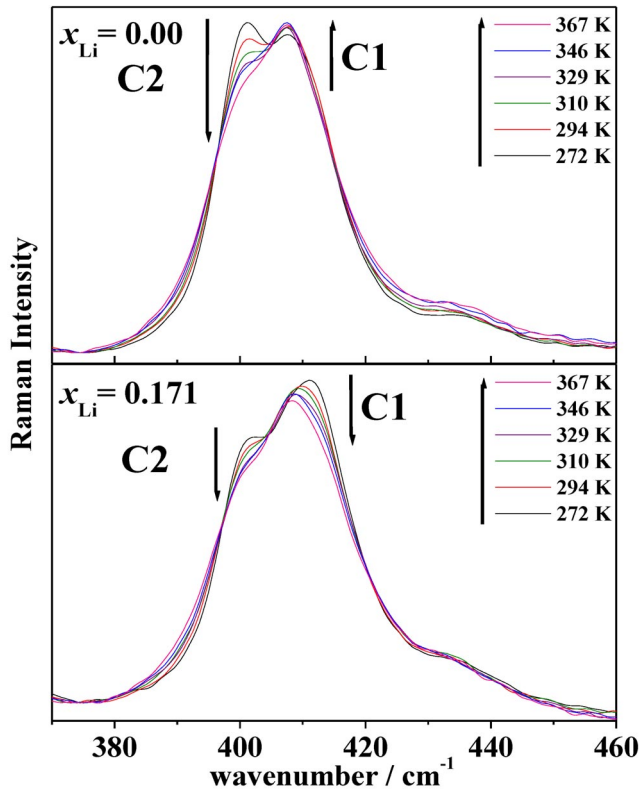

Fig. 6 Temperature dependence of Raman bands of BMI^+TFSA^-, with and without containing LiTFSA. The mole fraction of the lithium x_{Li} ion in the solution is given.

lithium ion. The apparent enthalpy can be rewritten as $\Delta H_{app}^\circ = \Delta H_{bulk}^\circ + x_{bound}(\Delta H_{bound}^\circ - \Delta H_{bulk}^\circ)$, and the ΔH_{app}° value is plotted against x_{bound} in Fig. 7. The ΔH_{app}° value indeed linearly decreases with increasing x_{bound}. By extrapolation, the ΔH_{bound}° value is evaluated from the intercept at $x_{bound} = 1$. The same applies also to the Gibbs energy and entropy for conformational change to obtain ΔG_{bound}° and ΔS_{bound}°. Table 2 summarizes the Gibbs energy, enthalpy, and entropy for the reaction $C_2 \rightleftharpoons C_1$ in the bulk and in the coordination sphere. The ΔG° value evidently shows that the equilibrium in the coordination sphere shifts to favorable formation of the C1 conformer. The enthalpy in the coordination sphere is negative and large, unlike that in the bulk. However, the C1 conformer is not favorable in the vicinity of the lithium ion according to theoretical molecular orbital (MO) calculation, despite the fact that

the dipole moment of the C1 conformer is significantly larger than that of the C2 conformer. The reason why the C1 conformer is favorable in the coordination sphere is thus unrevealed yet at the present stage. However, our recent studies imply that interactions of $Li(TFSA)_2^+$ in the second solvation sphere play an key role.

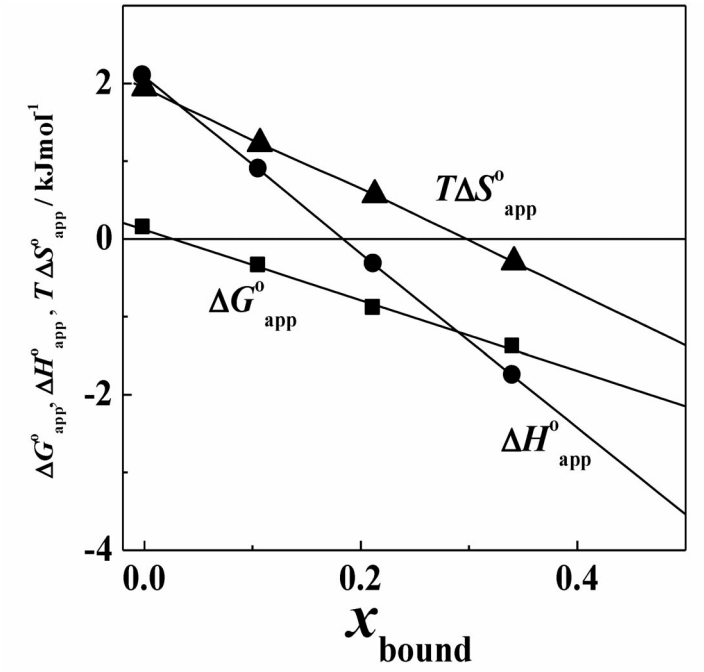

Fig. 7 Apparent thermodynamic parameters, $\Delta G_{app}°$, $\Delta H_{app}°$ and $T\Delta S_{app}°$/kJ mol^{-1}, at 298 K for the conformational equilibrium, C2 = C1, plotted against the mole fraction of $TFSA^-$ bound to the lithium ion x_{bound}.

Table 2 Thermodynamic parameters for the conformational equilibrium of $TFSA^-$, C2 = C1, in BMI^+TFSA^- (bulk) and in the solvation sphere of Li^+ (bound) at 298 K.

	Bulk	Bound
$\Delta G°$/kJ mol^{-1}	0.13(8)	–4.4(2)
$\Delta H°$/kJ mol^{-1}	2.08(5)	–9.2(1)
$T\Delta S°$/kJ mol^{-1}	1.9(2)	–4.6(3)

SOLVENT–SOLVENT INTERACTIONS

Physicochemical properties of solvent strongly depend on the liquid structure, or the solvent–solvent interaction. It has been known that the hydrogen-bonding interaction among solvent molecules creates a specific liquid structure in protic solvents. Indeed, a three-dimensional hydrogen-bonding network is formed among water molecules to lead to specific physicochemical properties of water. Also, a linear hydrogen-bonding linkage is formed among *N*-methylformamide molecules to lead to a very large dielectric constant in the liquid state. The hydrogen-bonding interaction may also occur among ions in protic ILs. With the $C_2H_5NH_3^+$-based ILs, the melting point of the ClO_4^-, BF_4^-, and $CF_3SO_2^-$ salts is

higher than 150 °C, and that of the CH_3COO^-, $H_2PO_4^-$, and $CH_3SO_4^-$ salts is above 100 °C, whereas that of the HF_2^- and NO_3^- salts is below 20 °C. The melting point of EAN, $C_2H_5NH_3^+NO_3^-$, seems abnormally low compared with that of other ethylammonium salts. As the ammonium group has an ability to form hydrogen bonds, the relatively low melting point might relate to a specific hydrogen-bonding structure of the salts in the crystalline and/or liquid states. Indeed, EAN has a layer structure in the crystalline state [39]. Physicochemical properties of ILs also may be related to their specific liquid and crystal structures, as well as normal molecular liquids. However, note that ILs are composed of bulky and flexible ions. Consequently, intramolecular interactions of an IL involve various types of atom–atom distances over a wide range, and extensively overlaps with the intermolecular interactions, it is thus difficult to extract the complicated liquid structure without the aid of theoretical molecular dynamics (MD) simulation. We thus combined the X-ray scattering experiment and theoretical MD simulation to reveal the liquid structure of EAN as follows [32].

The pair correlation function $G(r)$ of an IL is given as $G(r) = G_{intra}(r) + G_{inter}(r)$, where $G_{intra}(r)$ and $G_{inter}(r)$ denote pair correlation functions for intra- and intermolecular interactions, respectively. The experimental $G_{inter}(r)$ is extracted by subtracting $G_{intra}(r)$s of cation and anion, which are evaluated using crystal-structure data of the IL, from the observed $G(r)$. On the other hand, the calculated $G_{inter}(r)$ is directly obtained by an MD simulation by knowing atom positions at equilibrium. The $G_{inter}(r)$ consists of intermolecular cation–anion, cation–cation, and anion–anion interactions. If the calculated $G_{inter}(r)$ satisfactorily reproduces the experimental $G_{inter}(r)$, it may be possible to further discuss the partial atom–atom correlation $g(r)$ calculated on the basis of the MD simulation. Intermolecular interactions extracted by an X-ray scattering experiment are shown in Fig. 8, in terms of the radial distribution function $D(r)$-$4\pi r^2\rho_0$, in which positive and negative values represent higher and lower electron densities, respectively, relative to the average density over the whole space. The experimental $D(r)$-$4\pi r^2\rho_0$ (the dotted line) evidently shows that the electron density fluctuates over the range $r < 15$ Å, but it is rather difficult to assign a high-density peak to a given atom–atom correlation. An MD simulation is carried out for an *NTP* ensemble of 256 ion pairs of flexible $C_2H_5NH_3^+$ and NO_3^- ions with reliable pair potentials [32], and the calculated $D(r)$-$4\pi r^2\rho_0$ (the red line) reproduces well the peak positions. We then take into account the partial atom–atom correlation $g(r)$. The $g(r)$s between cation ($C_2H_5NH_3^+$) and anion (NO_3^-), between cations and between anions are respectively shown in Figs. 9a–c (with atom labeling, see ref. [32]). As seen, various atom–atom correlations overlap over the

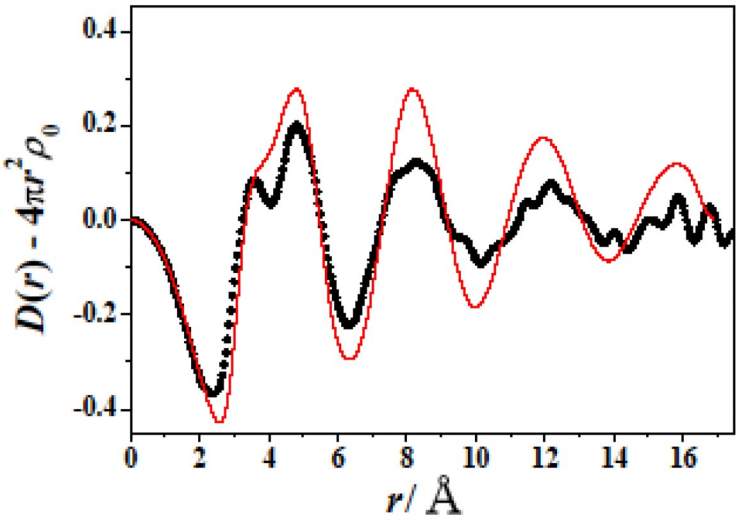

Fig. 8 Observed (dotted line) and calculated (red line) radial distribution functions, $D(r)$-$4\pi r^2\rho_0$, of EAN.

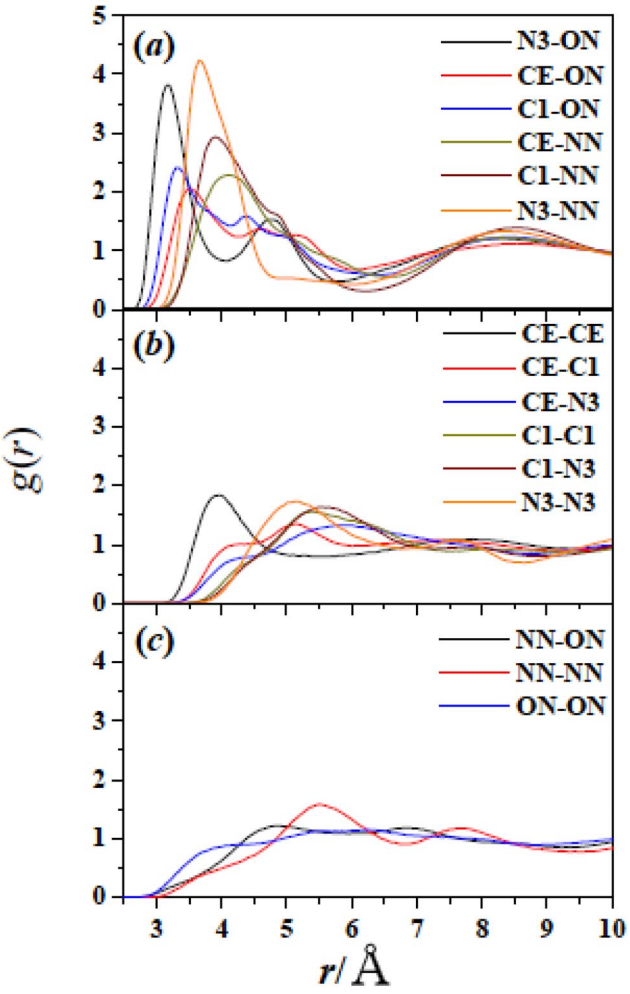

Fig. 9 Partial atom–atom correlations $g(r)$ between cation ($C_2H_5NH_3^+$) and anion (NO_3^-) (a), between cations (b) and between anions (c).

range, and it is difficult to allocate a given atom–atom interaction to observed peaks. In Fig. 9a, N3 and ON refer to the nitrogen atom of $C_2H_5NH_3^+$ and the oxygen atoms of NO_3^-, respectively. The N3–ON correlation shows two peaks at about 3.2 and 4.8 Å, which correspond to rather weakly hydrogen-bonded and non-bonded ON atoms of NO_3^-, respectively, to a given N3 atom. Similarly, the N3–NN correlation is atom–atom interactions between the N3 atom and the nitrogen atom (NN) of NO_3^-, and it shows a strong peak at 3.7 Å. Note that the atom–atom interaction between the N3 and bonded ON atoms (3.2 Å) is not largely different from that between the N3 and NN atoms (3.7 Å). Indeed, the difference (0.5 Å) is much smaller than the intermolecular NO bond length (1.25 Å) within the nitrate ion, indicating that the N3 atom locates above the nitrate plane with the N3···O–N angle of about 103º. This is consistent with the fact that the CE–ON and CE–NN correlations, where CE stands for the terminal carbon atom of $C_2H_5NH_3^+$, appear at 3.48 and 4.10 Å, respectively. The space distribution function (SDF) of oxygen atoms of the nitrate ion around the $C_2H_5NH_3^+$ ion is shown in Fig. 10, where a higher probability of the oxygen atom existence is shown by clouds. We see three holes around the $-NH_3^+$ group, which correspond to the space where the nitrogen atoms of nitrate ions are favorably located,

showing that three nitrate ions are bonded to the $–NH_3^+$ group with similar N3–ON and N3–NN distances. It is also seen that interaction between the ethyl group and the nitrate ion is weak, indicating that the cation–anion interaction occurs mainly through the polar $–NH_3^+$ group. This is indeed demonstrated by a snapshot at equilibrium in Fig. 11, where polar $–NH_3^+$ and NO_3^- groups are represented by red spheres and the alkyl groups by white. It is evident that EAN has a heterogeneous structure in the liquid state, in which polar groups contact each other to form polar channels, and the alkyl groups to form nonpolar domains, unlike a layer structure in the crystalline state.

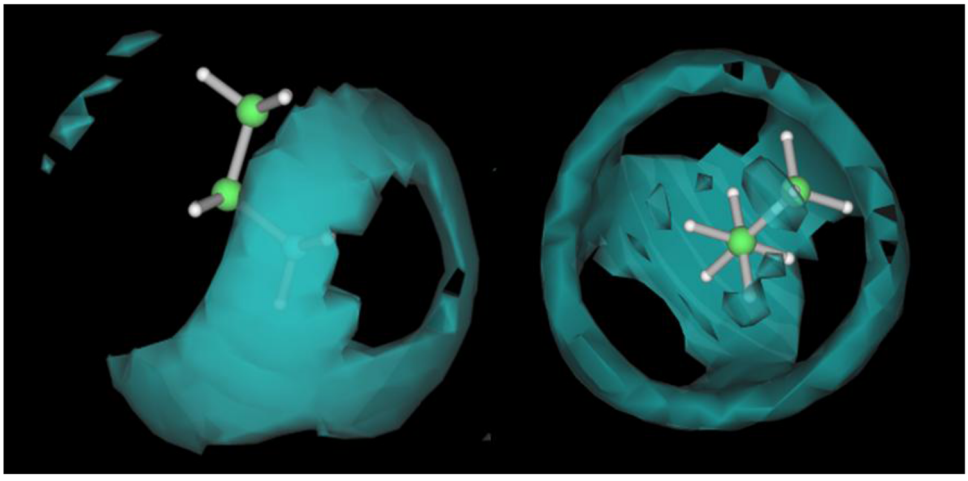

Fig. 10 SDF of oxygen atoms of the nitrate ion around the $–NH_3^+$ groups.

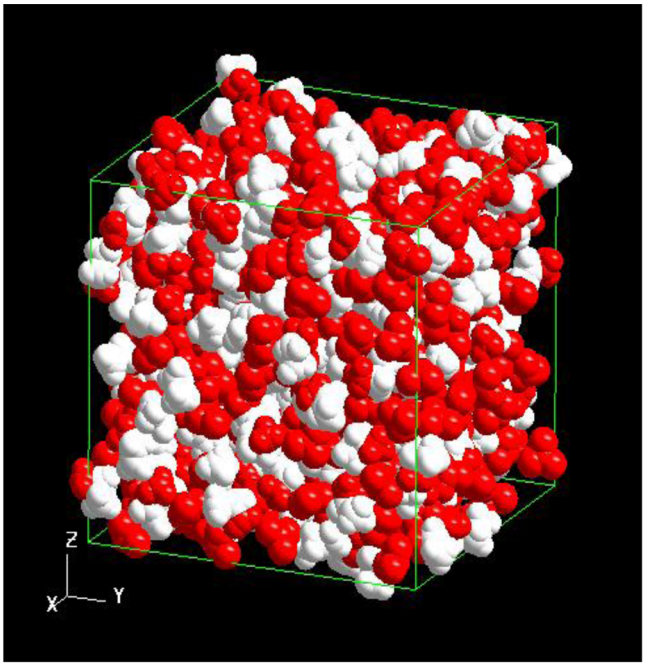

Fig. 11 Snapshot of the liquid structure of EAN at equilibrium, calculated using an MD simulation.

ACID–BASE PROPERTIES

EAN can be prepared by an acid–base reaction between nitric acid and ethylamine. The reaction is strongly exothermic, and is thus expected to give $C_2H_5NH_3^+$ and NO_3^- ions almost completely. However, in a protic solvent like water, solvent molecules partly dissociate proton to yield acid H_3O^+ and base OH^-. Similarly, protic EAN may dissociate proton according to the reaction, $C_2H_5NH_3^+ \rightarrow C_2H_5NH_2 + H^+$, and protons thus dissociated react with solvent anions according to $H^+ + NO_3^- \rightarrow HNO_3$. Therefore, it is supposed that a small amount of acid HNO_3 and base $C_2H_5NH_2$ molecules may be present in EAN. The autoprotolysis constant K_w (= $[H_3O^+][OH^-]$) is a measure of the acid–base strength of water, and the corresponding K_s for reaction 4 may be a measure of the acid–base strength in EAN.

$$C_2H_5NH_3^+ + NO_3^- \rightleftharpoons C_2H_5NH_2 + HNO_3 \quad (4)$$
$$K_s = [C_2H_5NH_2][HNO_3]$$

The pK_s value might be evaluated by ΔpK_a [13–15], the difference pK_a of HNO_3 and $C_2H_5NH_2$, in water as

$$\Delta pK_a = pK_a(C_2H_5NH_2) - pK_a(HNO_3) \quad (5)$$

However, note that it is an approximate value because the pK_a values are determined in water, where all species are hydrated. On the other hand, all species in EAN are solvated by counterions. Thus, we directly determined the K_s value by potentiometry using ISFET (ion-selective field effect transistor) or Pt electrodes, which may respond to HNO_3 as an acid [33]. An acidic EAN solution is prepared by adding HTFSA and a basic EAN solution by adding $EtNH_2$. Here, as HTFSA is a strong acid in EAN, it completely dissociates to give the nitric acid according to the reaction, HTFSA + NO_3^- = $TFSA^-$ + HNO_3, i.e., HNO_3 is the strongest acid in EAN. Thus, the acid–base reaction in EAN occurs according to the reaction, $C_2H_5NH_2 + HNO_3 \rightarrow C_2H_5NH_3^+ + NO_3^-$, i.e., the acid HNO_3 is neutralized by the base $EtNH_2$ to give the solvent ions, $C_2H_5NH_3^+$ and NO_3^-. Indeed, the titration curve shows a jump, and the pK_s value of 10 is obtained. This means that the pH value in neutral EAN is 5. The K_s values are also determined in EAN–water mixtures [34], and it is found that the value of 10.5 is kept practically unchanged over the wide range of EAN mole fraction x_{EAN} = 0.1–0.9.

Thermodynamic parameters for reaction 4 have been determined by calorimetry, and the results are summarized in Table 3, together with those in water, for comparison. The $\Delta G°$ is positive in both solvents, and is more positive in water, i.e., pK_w in water is larger than pK_s in EAN. On the other hand, the $\Delta H°$ in EAN is significantly more positive than that in water. Consequently, the $\Delta S°$ is negative in water, whereas it is positive in EAN. This may be expected as follows. In water, ions are generated according to $2H_2O \rightarrow H_3O^+ + OH^-$, and the strong solvation shell is thus created around the ions. It is supposed that the translational freedom of motion of solvent molecules is strongly hindered in the solvation shell. On the other hand, in EAN, the $-NH_3^+$ and NO_3^- groups are hydrogen-bonded to each other to form a channel-like network structure, and the translational freedom of motion of solvent ions must thus be hindered. The formation of neutral $C_2H_5NH_2$ and HNO_3 molecules in EAN may weaken the hydrogen-bonded network structure among solvent ions, which must enhance the translational freedom of motion of solvent ions to lead to increasing entropy. The positive $\Delta S°$ might be general in ILs in contrast to the negative $\Delta S°$ in molecular solvents.

Table 3 Thermodynamic parameters for the autoprotolysis reaction, $2H_2O = H_3O^+ + OH^-$, in water, and for the reaction, $C_2H_5NH_3^+ + NO_3^- = C_2H_5NH_2 + HNO_3$ in EAN.

	Water	EAN
$\Delta G°$/kJ mol^{-1}	79.9	56.1
$\Delta H°$/kJ mol^{-1}	56.5	83
$\Delta S°$/J K^{-1} mol^{-1}	–78.5	92

Once an accurate K_s value is obtained in an IL, the acid dissociation constant K_a can be determined in the IL. The acid dissociation constant has been determined for α-alanine in EAN. In Fig. 12, the average number of proton bound to α-alanine n_H is plotted against pH (= –log [HNO_3]) in EAN. The n_H in an EAN solution is experimentally given as

$$n_H = (C_H - [HNO_3] + K_s/[HNO_3])/C_L \quad (5)$$

where C_H and C_L denote total concentrations of dissociable proton and α-alanine, respectively, and the pH or –log[HNO_3] is measured by potentiometry. As seen, the n_H value is 2 at pH < 3, and it is 1 at pH > 6, and thus the first acid dissociation occurs in an acidic solution, as the neutral pH is 5 in EAN. The amino proton may not dissociate in EAN, unlike water. The pK_{a1} for the reaction, $NH_3^+CH(CH_3)COOH + NO_3^- \rightleftharpoons NH_3^+CH(CH_3)COO^- + HNO_3$, is given as

$$K_{a1} = [NH_3^+CH(CH_3)COO^-][HNO_3]/[NH_3^+CH(CH_3)COOH] \quad (6)$$

where [NO_3^-] is not barely expressed, because the concentration of the solvent NO_3^- is high and practically kept constant during the reaction. The K_{a1} value of 3.95 is obtained from the pH at n_H = 1.5. The K_{a1} value is 2.3 for the corresponding reaction, $NH_3^+CH(CH_3)COOH + H_2O \rightleftharpoons NH_3^+CH(CH_3)COO^- + H_3O^+$, in water. The larger K_{a1} value in EAN is not consistent with the fact that the basicity of H_2O is stronger than that of NO_3^-. In fact, it is found that the basicity of H_2O is

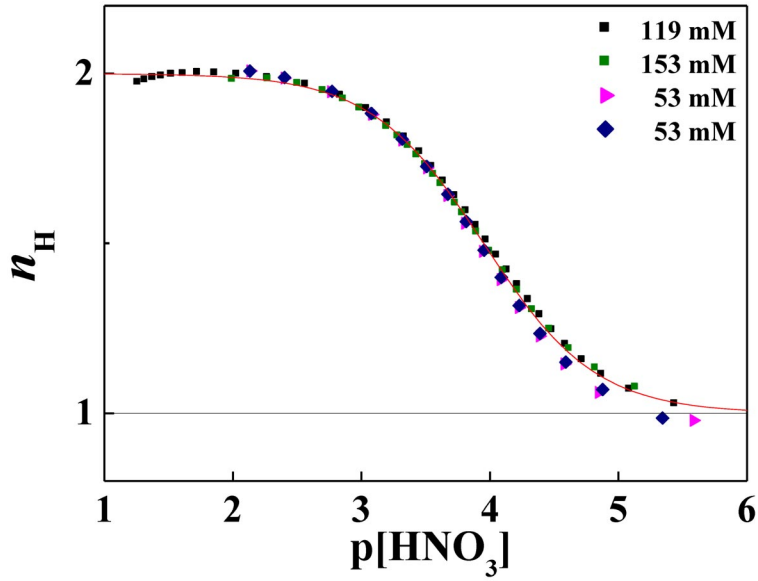

Fig. 12 Average number of proton bound to α-alanine, n_H plotted against pH (= –log [HNO_3]) in EAN.

slightly weaker than that of NO_3^- in EAN [34]. However, the extent is not so marked, and thus the pK_a difference cannot fully be ascribed to the basicity difference between the solvents. To clarify the nature of acid–base property in ILs, further experimental results are needed.

CONCLUSION

In this review, we summarized our recent results on solvation and conformational change of $TFSA^-$, and liquid structure and acid–base properties of a protic IL EAN. In EMI^+TFSA^-, divalent transition-metal ions, Mn^{2+}, Co^{2+}, Ni^{2+}, and Zn^{2+} are coordinated with three $TFSA^-$ ions, which chelate, as bidentate O donor ligand, to the transition-metal(II) ions. Similarly, the lithium ion is two-coordinated. $TFSA^-$ is a flexible molecule to give two stable conformers, *cis* (C1) and *trans* (C2), both of which are present in equilibrium in the coordination sphere, as well as in the bulk. It is found that the C2 conformer is more stable in the bulk, whereas the reverse is the case in the coordination sphere of the lithium ion.

The liquid structure of protic IL EAN in the liquid state has been revealed by combining X-ray scattering measurement and theoretical MD simulation. EAN has a heterogeneous liquid structure, in which polar $-NH_3^+$ and NO_3^- groups contact each other to form polar channels, and alkyl groups to form nonpolar domains. The $-NH_3^+$ group is weakly hydrogen-bonded with three NO_3^- ions through the oxygen atom. HNO_3 and $C_2H_5NH_2$ molecules behave as acid and base, respectively, in EAN. The acid–base strength K_s of EAN ($K_s = [HNO_3][C_2H_5NH_2]$), which corresponds to the autoprotolysis constant K_w of water, has been revealed to be pK_s = 10 by potentiometry. The enthalpy and entropy for the reaction have also been determined. On the basis of the K_s value, the acid dissociation constant K_a of the α-alanine in EAN has been obtained.

ACKNOWLEDGMENTS

This work has been financially supported by Grant-in-Aids for Scientific Research 19003963, 19350033, 19550022, 20350037 and for Scientific Research in Priority Area (Ionic Liquids) 20031024 from the ministry of Education, Culture, Sports, Science.

REFERENCES

1. J. Burgess. *Ions in Solution: Basic Principles of Chemical Interactions*, Harwood, Chichester (1999).
2. C. Reichart. *Solvents and Solvent Effects in Organic Chemistry*, VCH, New York (1988).
3. K. Fujii, T. Kumai, T. Takamuku, Y. Umebayashi, S. Ishiguro. *J. Phys. Chem.* **110**, 1798 (2006) and papers therein.
4. G. Mamantov, A. I. Popov (Eds.). *Chemistry of Nonaqueous Solutions: Recent Advances*, VCH, New York (1994).
5. P. Wasserscheid, T. Welton (Ed.). *Ionic Liquids in Synthesis*, Vols. 1 and 2, Wiley-VCH, Weinheim (2008).
6. M. Koel (Ed.). *Ionic Liquids in Chemical Analysis*, CRC Press, New York (2009).
7. J. F. Brennecke, R. D. Rogers, K. R. Seddon (Eds.). *Ionic Liquids IV*, American Chemical Society, Washington, DC (2007).
8. J. N. Canongia Lopes, A. A. H. Pádua. *J. Phys. Chem. B* **110**, 3330 (2006).
9. J. N. Canongia Lopes, M. F. C. Gomes, A. A. H. Pádua. *J. Phys. Chem. B* **110**, 16816 (2006).
10. A. Triolo, O. Russina, H.-J. Bluif, E. D. Cola. *J. Phys. Chem. B* **111**, 4641 (2007).
11. R. Atkin, G. G. Warr. *J. Phys. Chem. B* **112**, 4164 (2008).

12. Y. Umebayashi, R. Kanzaki, S. Ishiguro. *Encyclopedia of Surface and Colloid Science*, 3302 (2002).
13. C. A. Angell, N. Byrne, J.-P. Belieres. *Acc. Chem. Res.* **40**, 1228 (2007).
14. M. Yoshizawa, W. Xu, C. A. Angell. *J. Am. Chem. Soc*. **125**, 15411 (2003).
15. J.-P. Belieres, C. A. Angell. *J. Phys. Chem. B* **111**, 4926 (2007).
16. H. Ohno (Ed.). *Electrochemical Aspects of Ionic Liquids*, John Wiley, Hoboken (2005).
17. Y. Umebayashi, T. Fujimori, T. Sukizaki, M. Asada, K. Fujii, R. Kanzaki, S. Ishiguro. *J. Phys. Chem.* **109**, 8976 (2005).
18. S. Ishiguro, Y. Umebayashi, K. Fujii, R. Kanzaki. *Pure Appl. Chem*. **78**, 1595 (2006).
19. T. Fujimori, K. Fujii, R. Kanzaki, K. Chiba, H. Yamamoto, Y. Umebayashi, S. Ishiguro. *J. Mol. Liq.* **131–132**, 216 (2007).
20. K. Fujii, R. Kanzaki, T. Takamuku, T. Fujimori, Y. Umebayashi, S. Ishiguro. *J. Phys. Chem. B* **110**, 8179 (2006).
21. K. Fujii, Y. Umebayashi, S. Seki, S. Ishiguro. *J. Phys. Chem. B* **111**, 12829 (2007).
22. T. Sukizaki, S. Fukuda, K. Fujii, R. Kanzaki, K. Chiba, H. Yamamoto, Y. Umebayashi, S. Ishiguro. *Electrochemistry* **75**, 628 (2007).
23. J. N. Canongia Lopes, K. Shimizua, A. A. H. Pádua, Y. Umebayashi, S. Fukuda, K. Fujii, S. Ishiguro. *J. Phys. Chem. B* **112**, 1465 (2008).
24. K. Fujii, Y. Soejima, Y. Kyoshoin, S. Fukuda, R. Kanzaki, Y. Umebayashi, T. Yamaguchi, T. Takamuku, S. Ishiguro. *J. Phys. Chem. B* **112**, 4329 (2008).
25. K. Fujii, S. Shiro, S. Fukuda, T. Takamuku, Y. Umebayashi, S. Ishiguro. *J. Mol. Liq.* **143**, 64 (2008).
26. S. Fukuda, M. Takeuchi, K. Fujii, R. Kanzaki, T. Takamuku, K. Chiba, H. Yamamoto, Y. Umebayashi, S. Ishiguro. *J. Mol. Liq*. **143**, 2 (2008).
27. J. N. Canongia Lopes, K. Shimizua, A. A. H. Pádua, Y. Umebayashi, S. Fukuda, K. Fujii, S. Ishiguro. *J. Phys. Chem. B* **112**, 9449 (2008).
28. Y. Umebayashi, T. Mitsugi, K. Fujii, S. Seki, K. Chiba, H. Yamamoto, J. N. Canongia Lopes, A. A. H. Pádua, M. Takeuchi, R. Kanzaki, S. Ishiguro. *J. Phys. Chem. B* **113**, 4338 (2009).
29. Y. Umebayashi, T. Yamaguchi, S. Fukuda, T. Mitsugi, M. Takeuchi, K. Fujii, S. Ishiguro. *Anal. Sci.* **24**, 1297 (2008).
30. K. Fujii, T. Mitsugi, T. Takamuku, T. Yamaguchi, Y. Umebayashi, S. Ishiguro. *Chem. Lett.* **38**, 340 (2009).
31. R. Kanzaki, T. Mitsugi, S. Fukuda, K. Fujii, M. Takeuchi, Y. Soejima, T. Takamuku, T. Yamaguchi, Y. Umebayashi, S. Ishiguro. *J. Mol. Liq.* **147**, 77 (2009).
32. Y. Umebayashi, W. Chung, T. Mitsugi, S. Fukuda, M. Takeuchi, K. Fujii, T. Takamuku, R. Kanzaki, S. Ishiguro. *J. Comput. Chem. Jpn.* **7**, 125 (2008).
33. R. Kanzaki, K. Uchida, S. Hara, Y. Umebayashi, S. Ishiguro, S. Nomura. *Chem. Lett.* **36**, 684 (2007).
34. R. Kanzaki, K. Uchida, X. Song, Y. Umebayashi, S. Ishiguro. *Anal. Sci.* **24**, 1347 (2008).
35. K. Fujii, T. Nonaka, Y. Akimoto, Y. Umebayashi, S. Ishiguro. *Anal. Sci.* **24**, 1377 (2008).
36. A. Mudring, A. Babai, S. Arenz, R. Giernoth. *Angew. Chem., Int. Ed.* **44**, 5485 (2005).
37. Y. Umebayashi, T. Mitsugi, S. Fukuda, T. Fujimori, K. Fujii, R. Kanzaki, M. Takeuchi, S. Ishiguro. *J. Phys. Chem. B* **111**, 13028 (2007).
38. Y. Umebayashi, K. Fujii, S. Mori, S. Tsuzuki, S. Seki, K. Hayamizu, S. Ishiguro. *J. Phys. Chem. B* **114**, 6513 (2010).
39. Private communication with Dr. W. Henderson, North Carolina State University.

